Talanta 302 (2026) 129401

Contents lists available at ScienceDirect

Talanta

journal homepage: www.elsevier.com/locate/talanta

# A pH compensation and peak identification algorithm for voltammetric measurement of therapeutic drugs with sweat sensors

Robbert J. Nederhoff [a], Annemarijn S.M. Steijlen [a,b,*], Marc Parrilla [b], Jeroen Bastemeijer [a], Andre Bossche [a], Karolien De Wael [b]

[a] Electronic Instrumentation, Department of Microelectronics, Delft University of Technology, Mekelweg 4, Delft, 2628 CD, The Netherlands
[b] Antwerp Engineering, Photoelectrochemistry and Sensing (A-PECS), University of Antwerp, Groenenborgerlaan 171, Antwerp, 2020, Belgium

ARTICLE INFO

*Keywords:*
Therapeutic drug monitoring (TDM)
Wearable sensors
Sweat analysis
Voltammetry
Methotrexate
pH compensation
Interference removal
Gaussian fitting
Linear discriminant analysis

ABSTRACT

The current approach of Therapeutic Drug Monitoring (TDM) relies on blood analysis to closely monitor drugs with a narrow therapeutic window. This method is uncomfortable for the patient and time-consuming and therefore challenging for frequent monitoring. Electrochemical analysis in sweat is a promising alternative, as sweat sensors are non-invasive and can continuously measure drug concentrations. This study explores novel techniques to improve the analytical performance of voltammetric sensors for TDM in a sweat matrix. Methotrexate (MTX) is selected as the model analyte as it is a widely used therapeutic drug for treatment of cancer, rheumatoid arthritis, among other disorders. Changes in pH and interference from amino acids originating from sweat have been shown to impact the measurement of target drugs such as MTX. Herein, an algorithm is developed to compensate for potential pH fluctuations in sweat by using the relation between the pH level and the peak potential of the electro-oxidized analyte to estimate the pH and calculate the concentration of the analyte. Additionally, an algorithm was developed to separate peaks of distinct amino acids with a similar oxidation potential as MTX. The algorithm uses Gaussian fitting for subtracting and linear discriminant analysis (LDA) to identify the peak related to the analyte. The results demonstrate that the algorithms are effective for the detection of MTX and present an approach to compensating for sweat matrix-related interferences in wearable sweat sensors, driving development for low-cost continuous therapeutic drug monitoring.

## 1. Introduction

Therapeutic Drug Monitoring (TDM) is the clinical method of optimizing drug dosage to maximize therapeutic effectiveness while minimizing the risk of toxicity. It involves measuring the concentration of specific drugs in biological fluids, traditionally blood, where the concentration is correlated with the administered dose. TDM is particularly crucial for drugs with narrow therapeutic windows, where even minor fluctuations in drug concentration can lead to insufficient dosing or severe adverse effects [1]. Despite its clinical importance, current TDM methods are invasive for patients and have logistical challenges and high costs [2]. Sweat is a convincing alternative for TDM via blood. It is produced continuously and can reflect drug concentration changes over time, making it ideal for real-time monitoring through wearable technologies. A promising technique for wearable sensors is electrochemical sensing [3]. Among the various electrochemical techniques, voltammetry can be used to detect electroactive drugs in sweat without relying on recognition elements [4]. Square wave voltammetry allows for fast quantitative detection of a large range of substances [5,6]. However, there are also challenges in voltammetric sensing such as: (I) the submicromolar concentration of drugs in sweat [7,8], (II) temperature influences (although often relatively linear) [9], (III) interfering substances such as electrolytes, metabolites, drugs, trace metals, hormones, and proteins, that can cause redox peaks in the voltammogram, which may overlap with the peak from the analyte of interest [7], and (IV) Sweat pH, which can range from 2 to 8 [10], adds another layer of complexity. The pH of the matrix significantly influences the electrochemical behavior of many target drugs non-linearly, making it difficult to predict and compensate for these changes [11].

To overcome these challenges, several strategies have been developed. A common approach to remove interfering substances is to modify the electrode surface by adding functional coatings or altering the material composition to improve selectivity and sensitivity. These

* Corresponding author at: Electronic Instrumentation, Department of Microelectronics, Delft University of Technology, Mekelweg 4, Delft, 2628 CD, The Netherlands.
*E-mail addresses:* A.S.M.Steijlen@tudelft.nl (A.S.M. Steijlen), karolien.dewael@uantwerpen.be (K. De Wael).

https://doi.org/10.1016/j.talanta.2026.129401
Received 29 September 2025; Received in revised form 17 December 2025; Accepted 11 January 2026
Available online 21 January 2026

modifications can help shift the sensor's detection window away from regions where interfering substances are most active [12,13]. Another strategy employed for the pH variation in sweat involves buffering the solution to stabilize the pH before electrochemical analysis [14]. While these approaches have shown promising results, they are complex and would increase the cost and complexity of a wearable device.

Instead of physical solutions to tackle challenges originating from matrix pH influences and interfering substances, this article focuses on advanced digital approaches to derive the concentration of the analyte for the square wave voltammogram with varying pH. Approaches such as machine learning can be implemented to identify the analyte and its concentration, in the presence of interferents, based on the complete voltammogram. Techniques that have been implemented for voltammetric sensing range from straightforward linear regression to more complex models like neural networks to identifying and predicting concentrations of different analytes in vivo [15,16]. Other, more concise techniques such as principal component analysis (PCA) [17–21], partial least squares regression (PLSR) [22–24], support vector machines (SVM) [25,26] and linear discriminant analysis (LDA) are typically used for voltammogram feature extraction, such as peak voltage and current, and classification of undesirable molecules [18,27,28]. While all these approaches were considered, LDA was selected for peak classification due to its ability to rigorously separate two classes by features, such as peak current and potential, thus separating the analyte from interfering substances. Though both LDA and SVM are suitable for this task, LDA provides a more straightforward and effective solution for resolving overlapping peaks in this application by effortlessly multiplying the features with the LDA eigenvalues to classify the peaks [29].

This work presents new digital strategies to interpret square wave voltammograms for quantitative detection of pharmaceuticals in sweat with a varying pH and interfering substances present. The drug Methotrexate (MTX) is chosen as a first use case for development of the models. MTX was selected because TDM is widely applied for personalized MTX treatment of psoriasis, rheumatoid arthritis and cancer patients [30] and it is proven to be excreted in sweat [31]. First the voltammetric detection strategy of MTX in buffer is introduced. pH influences are mapped out and interfering substances in sweat are identified and characterized. Second, the algorithm for pH influences is presented and tested with samples of MTX in buffer solution at different pHs. In the third part, the algorithm for peak identification and quantification in the presence of interferents is explained and test results are shown. The fourth part presents the first validation study of the algorithms in real sweat samples spiked with MTX. The work concludes with the implementation of the voltammetric sensor and the new algorithms in a wearable system. Although traditionally matrix issues such as the interference of other substances are addressed with chemical changes of either the electrode surface or the buffers, this work focuses on improved digital interpretation of the voltammograms without chemical aids. The tailored algorithms developed in this work, using machine learning approaches, show promising results in improving the development of low-cost voltammetric sweat sensor systems for TDM.

## 2. Experimental section

### *Reagents and materials*

Methotrexate disodium (MTX) (99.35% purity) was purchased from Haihang Industry Co., (Shandong, China), and L-tryptophan was purchased from (Pharmacia & Upjohn Company, United States). The solutions were created using double-deionized water (18.2 MΩ/cm) (Milli-Q, Merck Millipore).

A phosphate-buffered saline (PBS) solution at pH 7.4 was prepared with potassium chloride and potassium phosphate from Sigma-Aldrich (Belgium), and Britton–Robinson buffer (20 mM) with pH levels of 2 to 8 were prepared with sodium borate, sodium acetate and sodium phosphate from Sigma-Aldrich (Belgium). 100 mM potassium chloride was added. The pH of the buffer solution was adjusted to the desired level using potassium hydroxide and hydrochloride solutions. The pH was measured with a pH meter (914 pH/Conductometer, model 2.914.0020, Metrohm, Herisau, Switzerland).

Voltammetry measurements were performed, and the sweat sample pH was measured (potentiometry) with custom-made screen-printed electrodes (SPEs) containing carbon (C2030519P4) working and counter electrodes and silver/silver chloride reference electrodes (C2040308P2) of Sun Chemical, United States. Polyethylene terephthalate (PET, 125 μm) was used as a substrate. For the pH measurement, the electrodes are modified with aniline and HCl (Sigma-Aldrich, Belgium) following the protocol as described in previous work [32].

Sweat samples were provided by healthy volunteers (male and female, 30–65 years old) during a regular 1.5 h outdoor running exercise. The skin was cleaned with deionized water and the sweat was collected using an absorbent patch (Cutisoft, BSN Medical, The Netherlands, collection area: 25 $cm^2$) that was covered with Parafilm (Sigma-Aldrich, Belgium) and attached to the skin at the medial lower back with Fixomull (BSN Medical, The Netherlands). The sweat was extracted from the absorbent with a 5 ml syringe and stored at −18 °C. Sweat tests were approved by the Human Ethics Research Committee of Delft University of Technology.

### *Instrumentation and apparatus*

Voltammetry and potentiometry were conducted using a MultiPalmSens4 and EmStat4R potentiostat (PalmSens, The Netherlands). Square wave voltammetry was performed within a potential range of −0.1 to 1.5 V, with a step potential of 5 mV, an amplitude of 25 mV, and a frequency of 10 Hz. The voltammetric measurements in buffers described in this manuscript contained 100 mM KCl solution.

### *Electrochemical analysis*

Matlab was utilized to analyze the data and develop the algorithms (MathWorks, United States).

### *Wearable system*

For this study, a wearable system has been developed. The potentiostat generally consists of a microcontroller controlling a negative feedback control loop and a transimpedance amplifier (TIA) connected with a digital-to-analog converter (DAC) generating the waveforms. The output is fed to an analog-to-digital converter (ADC) to the microcontroller for analysis [33]. This design is reproduced with the following components: STM32L432 microcontroller (STMicroelectronics, Switzerland), ADA4500-2 OPAMP (Analog Devices, United States), DAC70502 DAC (Texas Instruments, United States) and ADS7946 ADC (Texas Instruments, United States) assembled on a (printed circuit board) PCB and programmed with the STM32CubeIDE (STMicroelectronics, Switzerland). The system outputs the concentration via USB to a serial terminal on the PC.

## 3. Results and discussion

In the following section, we present and discuss the key findings of this study. First, the voltammetric detection of MTX is demonstrated and followed by an in-depth analysis of the impact of pH variations on the electrochemical response. Second, a novel compensation algorithm is introduced that corrects for variations in sweat pH. Additionally, the challenge of signal interference from amino acids is explored and a Gaussian fitting and linear discriminant analysis (LDA)-based approach for isolating the MTX signal is developed. The robustness of these algorithms is assessed using real sweat samples. Finally, the algorithms are implemented on a wearable system, and the feasibility of real-time therapeutic drug monitoring is discussed. The results highlight the potential of advanced digital processing techniques in the voltammetric detection of MTX with wearable sweat sensors.

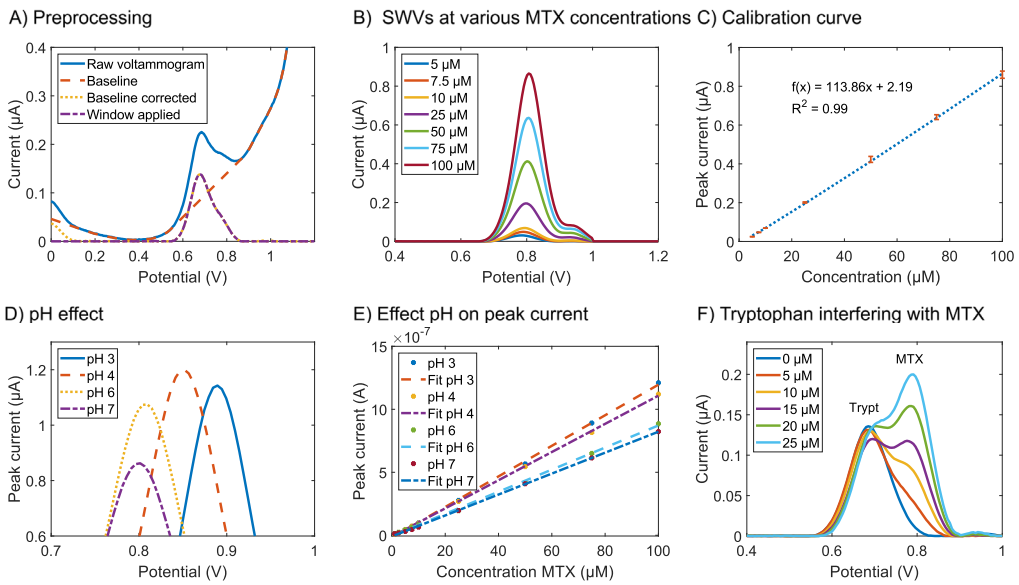


**Fig. 1.** Challenges of measuring MTX. (A) Pre-processed square wave voltammogram (SWV) of the antineoplastic drug methotrexate, which includes baseline compensation and selecting a detection window. (B) SWVs of increasing concentrations of MTX (5 μM–100 μM) in PBS 7.4. (C) The calibration curve shows a linear relationship between peak current and the concentration of MTX. (D) Effect of pH on the peak potential and peak current of 100 μM MTX in Britton-Robinson Buffer (pH 3–7). (E) The linear relationship of the peak current and the concentration of MTX at various pH levels. (F) Interferent study using 10 μM tryptophan as the main interferent in human sweat with various concentrations of MTX in PBS 7.4 with 0.1 M KCl. The resulting voltammograms highlight the peaks corresponding to both tryptophan and MTX.

### 3.1. Voltammetric detection of methotrexate

First, SWVs of MTX standards in PBS buffer pH 7.4 were recorded. Fig. 1A depicts the raw voltammogram of 5 μM MTX exhibiting an increased capacitive current upon increasing voltage. To obtain a clear view of the Faradaic currents occurring during the electrochemical oxidation of MTX, a preprocessing step is needed to enhance the sensing concept's analytical capabilities (Fig. 1A). A baseline compensation removes the capacitive current, which can differ slightly for every measurement and influence the measured peak current. The baseline compensation algorithm iteratively compares each point $a_i$ in the voltammogram with the average of its two neighboring points ($b_{avg}$) If $a_i$ is lower than $b_{avg}$, it remains unchanged; otherwise, it is replaced with $b_{avg}$. This process continues until no further points are updated or until a predefined maximum number of iterations is reached [34]. The window targets the redox process link to the analyte, and for MTX, it starts at 0.4 V and stops at 1 V. A continuous calibration of MTX in PBS 7.4 was performed from 5 μM to 100 μM (Fig. 1B). Fig. 1C shows the linear relation between the peak height and the concentration of MTX. The calibration curve using SPEs exhibits a slope of 0.00878 μA/μM, a LOD of 2.13 μM, a LOQ of 6.46 μM and excellent reproducibility of a maximum 4% standard deviation (SD) in peak current (N = 3). Mader et al. found a maximum concentration of MTX in sweat during high-dose therapy with MTX of around 3.7 μM (N = 5) [31]. The lowest concentration of 5 μM MTX in Fig. 1 is due to the reproducibility of the electrode, which limits the reliable measurement of concentrations below 5 μM MTX. Therefore, future work should include the application of electrode modifications to lower MTX detection limits and sensitivity.

The pH of human sweat can dramatically change depending on the physiological conditions of the person. Therefore, it is highly relevant to study the effect of pH on the MTX response as different pH in sweat can significantly affect the MTX measurement. Fig. 1D shows the peak current and potential shift of the MTX oxidation peak (100 μM) at different pHs (i.e. pH 3, 4, 6 and 7). The peak potential considerably shifts toward lower potential upon alkaline pHs. When performing a calibration curve at each pH condition, the linear relation between the peak current and the concentration is intact despite the changes in the slope and intercept (Fig. 1E). The slope and intercept between the varying pH levels have a non-linear relation, which probably originates from the deprotonation of MTX at 5.48 pKa [35], showing the complexity of pH effects on the voltammogram of MTX.

Another challenge with detecting MTX in sweat is the interference with other substances. The voltammogram of the amino acids tyrosine and tryptophan exhibits oxidation potentials similar to those of MTX (Fig. 1B and Figure S1). Changing concentrations of these amino acids in sweat increase the complexity of identifying the oxidation peaks originating from MTX. For our case study, tryptophan was selected as it is the closest electroactive interferent to the peak potential of MTX. Fig. 1F shows the voltammograms of binary mixtures of various concentrations of MTX and 10 μM tryptophan, which is the average concentration in sweat according to [36]. The amino acid has a slightly lower oxidation potential, resulting in overlapping peaks of MTX and tryptophan. The existing curve is a bell curve, a standard SWV curve with a shoulder on the left. As MTX increases, the peak related to MTX rises and becomes dominant. Thus, the oxidation process of this amino acid interferes with the voltammogram of MTX. An equivalent reaction occurs with tyrosine, but distinguishing it from MTX is easier, due to tyrosine's lower oxidation potential (Figure S1).

### 3.2. Compensation for pH effects

Compensating for pH effects of the sweat matrix is challenging due to the non-linear relationship between the slope and intercepts of the continuous calibration curves at different pH levels. The following strategy is developed: In step 1 (Fig. 2A), the voltammogram is recorded. Second, the voltammogram is preprocessed, using baseline correction (step 2 Fig. 2A). Subsequently, the pH is estimated using the peak potential, which exhibits a linear relation with different pH levels at a fixed MTX concentration (step 5 Fig. 2A and B). In step 6, Fig. 2A a lookup table is used to acquire the ratio between peak current and MTX concentration, corresponding to that pH level, and together with the peak current, the MTX concentration can be estimated (step 7 Fig. 2A). Notably, while the linear relation between the peak potential

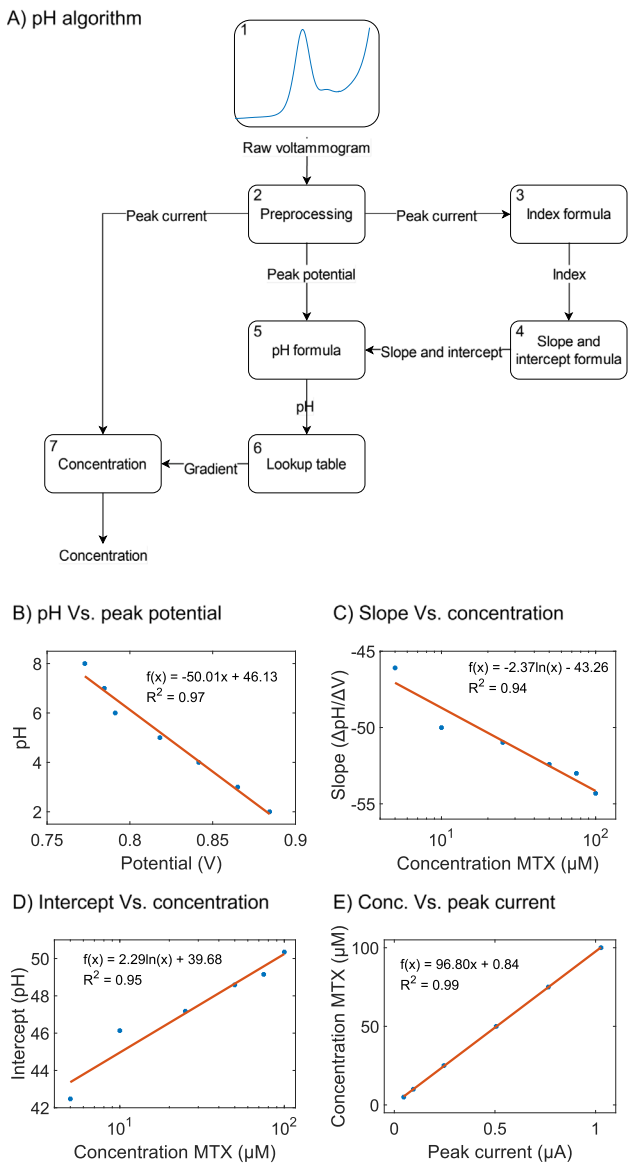


**Fig. 2.** pH Algorithm. (A) The algorithm determines the concentration using a voltammogram's peak current and peak potential. (B) The graph illustrates the relationship (both linear and logarithmic) between pH and the peak potential shift for 10 μM MTX. C and (D) Relationship between the slope and intercept with different concentrations of MTX. (E) The concentration can be estimated based on the magnitude of the peak current, averaged over the pH range of 2 to 8.

and pH holds for a fixed MTX concentration, there is a logarithmic relationship between the peak potential and pH across various MTX concentrations (Fig. 2C and D). This logarithmic relation is in steps 3 and 4 in Fig. 2A utilized for adjusting the pH due to higher or lower concentrations of MTX by using the peak current as an index (Fig. 2E) for the MTX concentration. Using these 7 steps, this algorithm can effectively compensate for the effect pH has on the MTX measurements. The implementation of the pH algorithm is provided in Listing 1 in the Supplementary Information.

The pH algorithm was tested using three SPEs with 7.5 μM MTX at pH 2 to 8. Based on the raw voltammograms, the pH level was predicted and the MTX concentration was calculated for each pH level at all SPEs. The absolute error between the known concentration of 7.5 μM MTX and the mean concentration derived by the algorithm was calculated (Table 1).

**Table 1**
pH algorithm 7.5 μM MTX estimation results of 3 SPEs.

| pH | SPE A (μM) | SPE B (μM) | SPE C (μM) | SD | Mean | Mean pH | Absolute error (μM) |
|---|---|---|---|---|---|---|---|
| 2 | 7.26 | 8.71 | 7.99 | 0.77 | 7.99 | 1.88 | 0.49 |
| 3 | 8.04 | 7.14 | 7.93 | 0.45 | 7.70 | 2.87 | 0.20 |
| 4 | 6.25 | 6.01 | 5.45 | 1.63 | 5.90 | 4.13 | 1.60 |
| 5 | 6.18 | 6.60 | 6.62 | 1.05 | 6.47 | 5.27 | 1.03 |
| 6 | 6.68 | 6.68 | 8.37 | 0.84 | 7.24 | 6.38 | 0.26 |
| 7 | 7.36 | 6.68 | 7.44 | 0.48 | 7.16 | 6.82 | 0.34 |
| 8 | 5.71 | 4.88 | 5.26 | 2.24 | 5.28 | 7.49 | 2.22 |

According to the results, the algorithm's estimation shows a good performance. The mean estimated concentration for all pHs is 6.82 μM with a SD of 0.98 μM. The highest error with respect to the known concentration is found at pH 4 and 5, which may originate from variations in electrode surface of the SPEs, measurement flaws, or a combination of both, which is similar for pH 8, where this results in a slightly off pH estimation. This results in a pH mismatch and lower concentration estimation. Despite these measurement and reproducibility errors, the algorithm itself remains reliable. This is supported by the fact that the pH conditions showing the largest concentration errors also show the highest deviation in the measurements. Therefore, the errors reflect limitations in the measurements rather than shortcomings of the algorithm. Nevertheless, the algorithm performs very well (errors below 0.5 μM) on the other pH estimations.

By including steps 3 and 4 of the pH algorithm, the algorithm estimates the pH 14% more accurately than without those steps. Further, step 6 contains a look-up table to select the ratio between peak current and MTX concentration for that pH level (Figure S2). Finding a representative relation is challenging due to the deprotonation of MTX, which arguably has a type of S-shape; however, more measurements at more pHs are necessary to confirm this trend and include it in the algorithm.

Overall, the algorithm shows good performance, and whenever a clear and measurable signal is obtained, the algorithm reliably calculates the pH and MTX concentration, indicating that the method is limited by the in-house screen-printed electrodes. Thus, the algorithm could become more robust and accurate when increasing (i) the reproducibility of the SPEs and by finetuning the SPE fabrication process (ii) adding extra pH measurements to improve the look-up table to enhance the accuracy in estimating the MTX concentration at different pH levels.

### 3.3. Peak identification in the presence of interferents

Sweat is an interesting biofluid rich in physiological information. Sweat can contain levels of therapeutic drugs as well as other biomolecules that can interfere with the sensing of the analyte of interest. First, a research into the state of the art showed that tyrosine and tryptophan are present in sweat at μM levels [36] and oxidation reactions of these substances will potentially interfere with the oxidation of MTX [12]. To verify this assumption, square wave voltammetry was performed with sweat samples obtained from subjects by the absorbent patch method during the sports exercise (Figure S5). The SWV profile showed redox peaks at 0.716 V and 0.691 V, potentially due to the electro-oxidation of amino acids at the carbon SPE around pH 7.4. To verify this, standards of 50 μM of the possible electroactive interferents (tryptophan, methionine, tyrosine, histidine, cysteine, proline, ascorbic acid, uric acid) in acetate buffer with pH 5 were analyzed with the SPE. Figure S1 shows that ascorbic acid, uric acid, tryptophan and tyrosine showed prominent peaks in the recorded potential window. Tryptophan and Tyrosine showed peaks (at 0.77 V and 0.75 V) that overlap with the peak potential window of MTX at pH 7.4 (mean 0.78 V from 1 to 100 μM). Additionally, tryptophan and tyrosine were mixed with MTX to assess their interference in PBS at pH 7.4 (Figure S1B), revealing significant overlap with MTX. To enable reliable quantitative detection

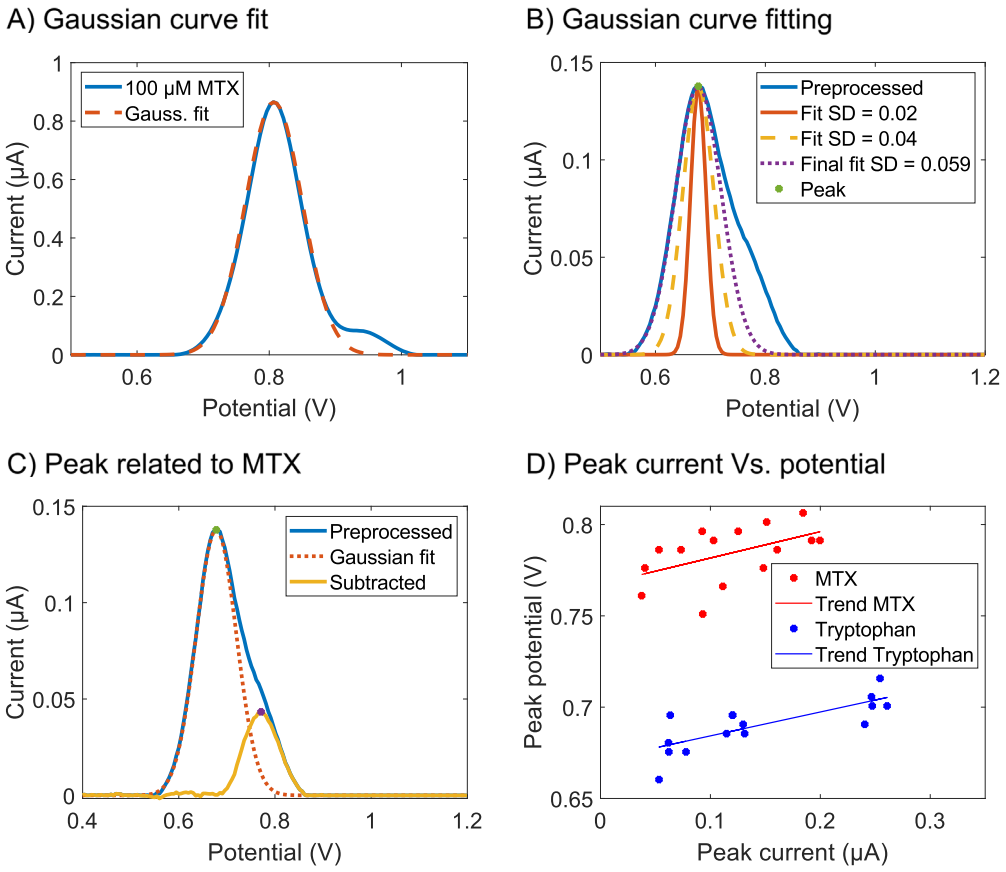


**Fig. 3.** Interference algorithm. (A) The voltammograms of 100 µM MTX in PBS at pH 7.4 with 0.1 M KCl show a perfect Gaussian fit. (B) Gaussian fit procedure of 10 µM Tryptophan and 5 µM MTX at pH 7.4 with 0.1 M KCl. (C) Fitted Gaussian and the curve related to 5 µM MTX, which is the Gaussian subtracted from the pre-processed voltammogram. (D) The peak location of the peaks related to MTX and tryptophan.

of MTX in the presence of these interferents, a tailored algorithm was made. The main advantage of the proposed algorithm is that it is specifically made for analyte detection in sweat. Most existing algorithms do not account for varying pH conditions and the presence of sweat interferents. Unlike existing methods, our algorithm integrates baseline correction, interference removal (via LDA), and pH compensation in a single framework. This enables more reliable identification of the MTX peak under realistic, variable sweat conditions. Fig. 1F shows the SWV of tryptophan with MTX, resulting in an overlapping signal with two peaks or a shoulder. The location of the shoulder peak in the voltammogram can be identified by differentiating the voltammogram once or twice (Figure S3). The resulting shoulder height identified by the derivative can be used to estimate the MTX concentration. Another method is to fit a Gaussian curve. An algorithm is developed to fit a Gaussian curve on SWVs of varying tryptophan concentrations and identify the MTX concentration. Fig. 3A shows that 100 µM MTX nearly flawlessly fits a Gaussian curve. The Gaussian formula consists of the amplitude, shift, and width of the curve. Fig. 3B shows the procedure for fitting a Gaussian curve on a signal. First, the dominant peak is located for the amplitude and shift for the curve fitting. Secondly, the width or standard deviation of the Gaussian is increased during iterations until it reaches the boundary of the signal. Third, the curve is subtracted from the signal, resulting in a curve related to the MTX concentration (Fig. 3C). The peak height of the related MTX curve gives a valid estimation of the MTX concentration. The last part of the procedure is to identify the peak of MTX with linear discriminant analysis (LDA).

LDA is a machine-learning algorithm that maximizes the ratio of overall variance to within-class variance to expand the separation between classes. In the training data, tryptophan and MTX are the classes, and the peak currents and potentials are the features. The peak potential is an applicable parameter because MTX has a higher peak potential than tryptophan and tyrosine. However, increasing concentrations in both MTX and tryptophan show an increase in both the peak current and peak potential (Fig. 1B). The peak current can, therefore, be utilized differentiate to increase the spread between MTX and tryptophan (Fig. 3D). Moreover, LDA uses the between-class variance, the same as the covariance of the data set whose members are the mean vectors of each class, and the mean sum of the classes' covariance matrices. LDA divides these matrices to maximize the separation [29]. Projecting the data onto the significant eigenvector of the new matrix divides the data (Figure S4). New data is multiplied with this vector to classify it as MTX or tryptophan. The algorithm uses the coefficients of the linear equation of Fig. 1C to transform the peak currents to concentration MTX.

The interference algorithm is applied to the measurements of three SPEs varying in MTX and tryptophan. The tryptophan range is according to the concentrations in sweat [36]. The LDA algorithm is trained on the mean values from the first 15 measurements. After that, it is applied to the individual electrodes and shows 100% accuracy in identifying MTX. To validate the algorithm, a verification set is made (the last five measurements in Table 2), where the algorithm can successfully separate and identify the MTX-related peaks. The implementation of the interference algorithm is provided in Listing 2 in the Supplementary Information.

The Gaussian fitting algorithm adds additional complexity but is preferred over the approach that uses derivative(s) to identify the shoulder. This last technique introduces additional challenges as well, mainly due to the increased noise in both the first and second derivatives. Developing an algorithm that first smooths the signal before locating the shoulder, especially in the presence of multiple local

**Table 2**
Results interference algorithm.

| Concentration tryptophan (μM) | Concentration MTX (μM) | SPE A (μM) | SPE B (μM) | SPE C (μM) | SD | Mean | Absolute error (μM) |
|---|---|---|---|---|---|---|---|
| | 5 | 6.19 | 7.36 | 7.40 | 1.19 | 6.99 | 1.99 |
| | 10 | 12.99 | 12.55 | 13.86 | 1.84 | 13.13 | 3.13 |
| 5 | 15 | 14.94 | 14.69 | 14.95 | 0.11 | 14.86 | 0.14 |
| | 20 | 19.35 | 19.29 | 18.92 | 0.48 | 19.19 | 0.81 |
| | 25 | 23.98 | 25.01 | 23.44 | 0.62 | 24.14 | 0.86 |
| | 5 | 7.22 | 7.12 | 7.77 | 1.38 | 7.37 | 2.37 |
| | 10 | 10.44 | 10.57 | 10.71 | 0.34 | 10.58 | 0.58 |
| 10 | 15 | 15.66 | 13.79 | 12.41 | 0.98 | 13.95 | 1.05 |
| | 20 | 20.35 | 20.69 | 20.73 | 0.35 | 20.59 | 0.59 |
| | 25 | 25.00 | 25.20 | 24.76 | 0.11 | 24.98 | 0.02 |
| | 5 | 7.47 | 9.37 | 10.83 | 2.56 | 9.22 | 4.22 |
| | 10 | 14.93 | 12.03 | 14.31 | 2.28 | 13.76 | 3.76 |
| 20 | 15 | 17.52 | 17.97 | 14.05 | 1.34 | 16.51 | 1.51 |
| | 20 | 23.18 | 21.83 | 15.98 | 1.81 | 20.33 | 0.33 |
| | 25 | 33.21 | 27.07 | 20.25 | 3.24 | 26.84 | 1.84 |
| 15 | 5 | 7.65 | 8.94 | 8.86 | 2.04 | 8.48 | 3.48 |
| 5 | 15 | 16.36 | 16.69 | 16.64 | 0.91 | 16.56 | 1.56 |
| 7.5 | 7.5 | 8.72 | 9.61 | 10.18 | 1.21 | 9.50 | 2.00 |
| 15 | 15 | 16.29 | 17.62 | 18.09 | 1.42 | 17.33 | 2.33 |
| 20 | 25 | 25.76 | 27.52 | 26.69 | 1.04 | 26.66 | 1.66 |

minima and maxima, further complicates the process. After smoothing, the derivative is applied to identify the peak or shoulder height related to MTX. Hereafter, the concentration of MTX can be calculated using the coefficients of the linear equation shown in Fig. 1C. However, a challenge arises when dealing with low MTX concentrations (e.g. 5 μM) and high tryptophan concentrations (e.g. 15 μM), where the shoulder may not be detected due to the derivative showing no local minima or maxima, probably due to a low signal to noise ratio. For the Gaussian fit (Table 2), the error is generally for low concentrations MTX and high concentrations tryptophan incorrect, similar to the problems the derivative detection faces. However, the error in this approach is significantly higher than the Gaussian fit algorithm, underscoring the exactness of the latter (Table S2).

Overall, the Gaussian fit algorithm proved to work when peaks partially overlap, and a shoulder is perceptible or when there are two peaks. It shows excellent results with low error at higher concentrations. The larger absolute errors mainly occur in samples with low MTX concentrations and high tryptophan levels, where the peak separation becomes unreliable. In addition, the variability between electrodes affects reproducibility, which also results in occasional higher average error. Further research is required for concentrations lower than 5 μM MTX, usually found in sweat. However, in cases where the electrodes produced a clear and measurable MTX-related signal, the algorithm successfully identified the peak. This means the algorithm is already capable of handling lower concentrations if the input signal quality is sufficient. In future work, the in-house screen-printing process should be further optimized to achieve reliable measurements below 5 μMM. This can be accomplished by increasing electrode sensitivity and reproducibility, for example by using higher-quality prints with larger surface area and improved surface consistency. Additionally, changing the pH affects the peak potential (Fig. 1D pH effects). In this study, the results are obtained from tryptophan and MTX at pH 7.4. Unfortunately, for tryptophan, peak potential shift due to pH does not have a similar relation as that of MTX, resulting in perfectly aligned peaks around pH 6 (Figure S6). The algorithm cannot yet differentiate between the two, and other techniques should be employed. A possible solution is to use a buffer reservoir to change the pH of the sweat before applying electrochemical analysis, similar to the method described in literature [32].

### 3.4. Validation with sweat samples

Sweat was spiked with MTX to validate the pH and interference algorithms together. First, the voltammogram is preprocessed. Second, the Gaussian fitting algorithm extracts the MTX-related peak. Last, the pH algorithm estimates the pH from the peak potential and uses this to select the proper slope to calculate the MTX concentration. Fig. 4A shows a sweat sample with pH 7.35 and 5 μM MTX. Fig. 4B and C show the same sweat sample spiked with 10 μM MTX spiked but with different electrodes. Finally, in Fig. 4D, 10 μM MTX was spiked in another sweat sample. The sweat samples had slightly different pH levels, 7.35 and 7.51. Nevertheless, the figures show a similar curve to the solution with tryptophan and MTX in buffer, including an MTX-related shoulder.

The Gaussian algorithm effectively fits a Gaussian curve to the signal, subtracting it to isolate the MTX-related peak, which LDA accurately identifies across all four figures. However, the fit indicates that the sweat sample deviates slightly from an ideal Gaussian curve compared to the buffer, probably due to other components in sweat, such as tyrosine, which has a lower peak potential. Despite this variation, the MTX-related peak height is according to the peak height in the buffer. Following the Gaussian fit, the pH algorithm is employed, estimating pH values of 7, 7, 8, and 8, respectively. It then calculates the MTX concentrations as 5.02, 7.66, 11.19, and 9.36 μM, with an absolute error of 0.02, 2.44, 1.19 and 0.64 μM, demonstrating the algorithm's potential. Although this is relatively accurate for these samples, sweat composition can vary, such as the NaCl concentration, which deviates between 10 and 90 mM [37,38], shifting the peak potential according to the Nernst equation (Figure S7). Although this shift is at a maximum 50 mV, it can increase the errors of the concentration estimation. Furthermore, the peak height can vary based on temperature fluctuations (0.1 μA, between 30° and 35° Celcius, Figure S8). Further research is necessary to enhance the algorithm's robustness across diverse sweat samples and refine its accuracy, in different physiological and environmental situations.

### 3.5. Implementation on wearable

The voltammogram of sweat sample 1 SPE A, spiked with 10 μM MTX, has been uploaded to the wearable (Figure S9). The wearable device has been specially developed for this research to investigate if the algorithms can be executed on a small, low-cost, low-power microprocessor. The wearable can perform an SWV, whereafter the algorithms compute the molar concentration and output it via USB to a serial monitor. The wearable executes the baseline compensation, a relatively intensive algorithm that goes through the voltammogram

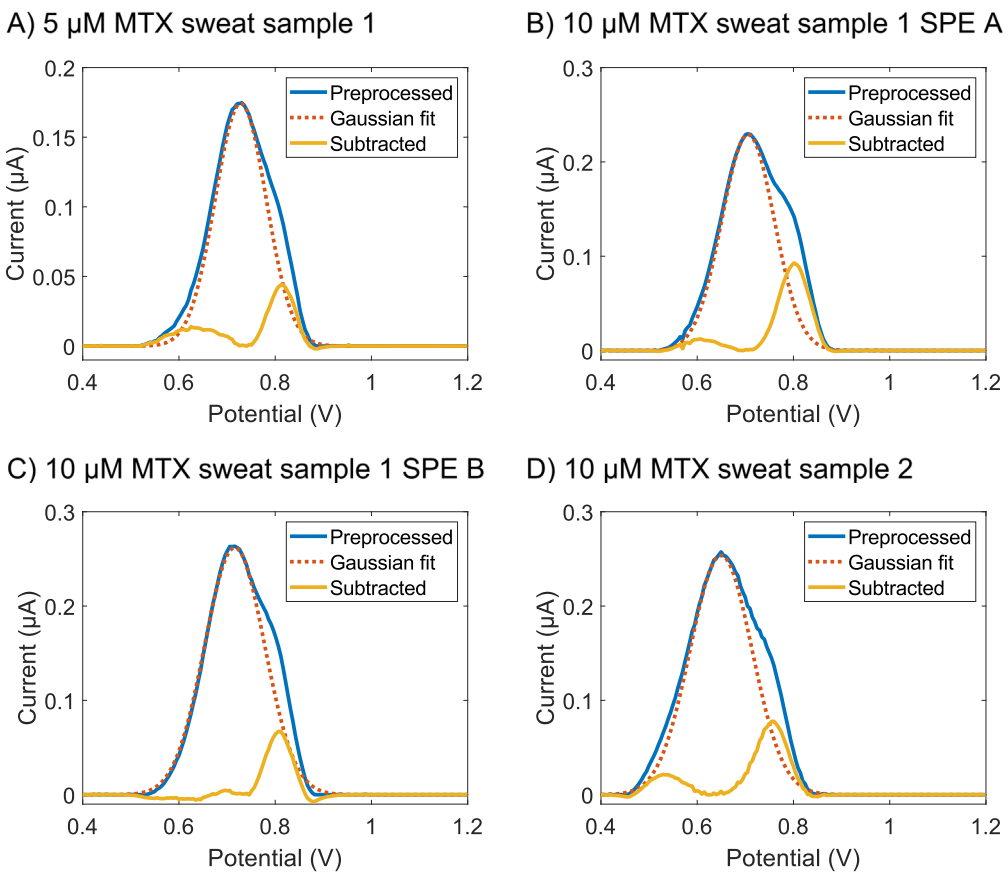


**Fig. 4.** Validation of the algorithm using sweat samples. (A) Voltammogram of sweat sample 1 spiked with 5 µM MTX. B and (C) Voltammograms from different electrodes of sweat sample 1 spiked with 10 µM MTX. (D) Voltammogram of sweat sample 2 spiked with 10 µM MTX.

several 100 times to remove the baseline. Second, a window is applied to remove other possible interferences. Third, the peak current is obtained. Together with the peak potential, they are required for the Gaussian fit algorithm that removes the influence of amino acids and leaves a peak related to the MTX concentration. At last, the pH algorithm compensates for the pH shift (Figure S10).

The result is that the algorithm estimates the pH at 6.2 and the concentration at 9.26 µM, which differs from the algorithms implemented in MatLab. Presumably, there is some loss due to the conversions in data for the microcontroller and the calculation of the algorithms with it, which needs further optimizations. Nevertheless, the estimated concentration is still reasonably accurate, and the wearable performs all the algorithms in less than 200 ms at a clock speed of 80 MHz. These results demonstrate that the algorithms can be effectively executed on an embedded system, enabling real-time sweat analysis, indicating significant progress in developing wearable sensors for therapeutic drug monitoring.

## 4. Conclusion

In conclusion, this paper has demonstrated several approaches of overcoming challenges in voltammetric detection of drugs in complex matrices such as sweat. The focus was on developing intelligent algorithms to compensate for pH variations and remove effects from interferents. These algorithms can run on wearable systems and improve the accuracy of voltammetric sensors, while maintaining affordability. Gaussian fitting and LDA were used to separate interfering amino acids in sweat to identify peaks related to the analyte Metrothexate (MTX). The Gaussian fit algorithm effectively separated peaks and identified the peak associated with the analyte. For pH compensation, the pH is estimated using the relation between the MTX oxidation peak potential and the pH and the relationship between peak current and MTX concentration at different pH levels is used, to increase the accuracy of the algorithm. The algorithms were tested with real sweat samples and even implemented on a wearable. Results showed successful estimation of MTX concentrations in sweat around 10 µM MTX at a pH between 7 and 8. Overall, the presented algorithms show an innovative approach to compensate for pH and interference effects, towards accurate voltammetric detection of electroactive drugs in sweat, which can be employed for new TDM methods.

## CRediT authorship contribution statement

**Robbert J. Nederhoff:** Visualization, Validation, Software, Methodology, Investigation, Formal analysis, Data curation, Conceptualization. **Annemarijn S.M. Steijlen:** Writing – review & editing, Writing – original draft, Supervision, Methodology, Investigation, Conceptualization. **Marc Parrilla:** Writing – review & editing, Methodology, Conceptualization. **Jeroen Bastemeijer:** Writing – review & editing, Supervision, Methodology. **Andre Bossche:** Writing – review & editing, Supervision, Methodology. **Karolien De Wael:** Writing – review & editing, Supervision, Funding acquisition.

## Declaration of competing interest

The authors declare that they have no known competing financial interests or personal relationships that could have appeared to influence the work reported in this paper.

## Acknowledgments

A. S. acknowledges funding through a Rubicon fellowship from the Dutch Research Council (File No. 019.223EN.003). K.D.W. acknowledges funding from UAntwerp (BOF and IOF) and FWO-Flanders.

## Appendix A. Supplementary data

Supplementary material related to this article with additional electrochemical measurement results, algorithm related data and information about the wearable, can be found online at: https://doi.org/10.1016/j.talanta.2026.129401.

## Data availability

Data will be made available on request.

## References

[1] A. Dasgupta, Introduction to therapeutic drug monitoring: Frequently and less frequently monitored drugs, in: Therapeutic Drug Monitoring, Elsevier, 2024, pp. 1–35.
[2] E. Fu, K. Khederlou, N. Lefevre, S.A. Ramsey, M.L. Johnston, L. Wentland, Progress on electrochemical sensing of pharmaceutical drugs in complex biofluids, Chemosensors 11 (8) (2023) 467.
[3] M. Parrilla, U. Detamornrat, J. Domínguez-Robles, S. Tunca, R.F. Donnelly, K. De Wael, Wearable microneedle-based array patches for continuous electrochemical monitoring and drug delivery: toward a closed-loop system for methotrexate treatment, ACS Sensors 8 (11) (2023) 4161–4170.
[4] S. Lin, B. Wang, W. Yu, K. Castillo, C. Hoffman, X. Cheng, Y. Zhao, Y. Gao, Z. Wang, H. Lin, et al., Design framework and sensing system for noninvasive wearable electroactive drug monitoring, ACS Sensors 5 (1) (2020) 265–273.
[5] B. Uslu, S.A. Ozkan, Electroanalytical methods for the determination of pharmaceuticals: a review of recent trends and developments, Anal. Lett. 44 (16) (2011) 2644–2702.
[6] V.K. Gupta, R. Jain, K. Radhapyari, N. Jadon, S. Agarwal, Voltammetric techniques for the assay of pharmaceuticals—a review, Anal. Biochem. 408 (2) (2011) 179.
[7] F. Gao, C. Liu, L. Zhang, T. Liu, Z. Wang, Z. Song, H. Cai, Z. Fang, J. Chen, J. Wang, et al., Wearable and flexible electrochemical sensors for sweat analysis: a review, Microsystems & Nanoeng. 9 (1) (2023) 1–21.
[8] K.K. Yeung, T. Huang, Y. Hua, K. Zhang, M.M. Yuen, Z. Gao, Recent advances in electrochemical sensors for wearable sweat monitoring: A review, IEEE Sensors J. 21 (13) (2021) 14522–14539.
[9] Y. Yang, Y. Song, X. Bo, J. Min, O.S. Pak, L. Zhu, M. Wang, J. Tu, A. Kogan, H. Zhang, et al., A laser-engraved wearable sensor for sensitive detection of uric acid and tyrosine in sweat, Nature Biotechnol. 38 (2) (2020) 217–224.
[10] A.B. Stefaniak, C.J. Harvey, Dissolution of materials in artificial skin surface film liquids, Toxicol. Vitr. 20 (8) (2006) 1265–1283.
[11] P.A. Raymundo-Pereira, N.O. Gomes, S.A. Machado, O.N. Oliveira Jr., Wearable glove-embedded sensors for therapeutic drug monitoring in sweat for personalized medicine, Chem. Eng. J. 435 (2022) 135047.
[12] S. Lin, W. Yu, B. Wang, Y. Zhao, K. En, J. Zhu, X. Cheng, C. Zhou, H. Lin, Z. Wang, et al., Noninvasive wearable electroactive pharmaceutical monitoring for personalized therapeutics, Proc. Natl. Acad. Sci. 117 (32) (2020) 19017–19025.
[13] H. Li, Z. Deng, Z. Jiao, R. Zhu, L. Ma, K. Zhou, Z. Yu, Q. Wei, Engineering a au-NPs/nafion modified nanoporous diamond sensing interface for reliable voltammetric quantification of dopamine in human serum, Chem. Eng. J. 446 (2022) 136927.
[14] S. Tajik, H. Beitollahi, S. Shahsavari, F.G. Nejad, Simultaneous and selective electrochemical sensing of methotrexate and folic acid in biological fluids and pharmaceutical samples using Fe3O4/ppy/Pd nanocomposite modified screen printed graphite electrode, Chemosphere 291 (2022) 132736.
[15] U. Hoss, E.S. Budiman, H. Liu, M.P. Christiansen, Continuous glucose monitoring in the subcutaneous tissue over a 14-day sensor wear period, J. Diabetes Sci. Technol. 7 (5) (2013) 1210–1219.
[16] G.H. Matsushita, A.H. Sugi, Y.M. Costa, A. Gomez-A, C. Da Cunha, L.S. Oliveira, Phasic dopamine release identification using convolutional neural network, Comput. Biol. Med. 114 (2019) 103466.
[17] M. Falk, E.J. Nilsson, S. Cirovic, B. Tudosoiu, S. Shleev, Wearable electronic tongue for non-invasive assessment of human sweat, Sensors 21 (21) (2021) 7311.
[18] M. Palit, B. Tudu, P.K. Dutta, A. Dutta, A. Jana, J.K. Roy, N. Bhattacharyya, R. Bandyopadhyay, A. Chatterjee, Classification of black tea taste and correlation with tea taster's mark using voltammetric electronic tongue, IEEE Trans. Instrum. Meas. 59 (8) (2009) 2230–2239.
[19] M.L. Heien, M.A. Johnson, R.M. Wightman, Resolving neurotransmitters detected by fast-scan cyclic voltammetry, Anal. Chem. 76 (19) (2004) 5697–5704.
[20] M.D. Nguyen, S.T. Lee, A.E. Ross, M. Ryals, V.I. Choudhry, B.J. Venton, Characterization of spontaneous, transient adenosine release in the caudate-putamen and prefrontal cortex, PLoS One 9 (1) (2014) e87165.
[21] A.E. Ross, B.J. Venton, Sawhorse waveform voltammetry for selective detection of adenosine, ATP, and hydrogen peroxide, Anal. Chem. 86 (15) (2014) 7486–7493.
[22] C.J. Meunier, G.S. McCarty, L.A. Sombers, Drift subtraction for fast-scan cyclic voltammetry using double-waveform partial-least-squares regression, Anal. Chem. 91 (11) (2019) 7319–7327.
[23] C.S. Movassaghi, K.A. Perrotta, H. Yang, R. Iyer, X. Cheng, M. Dagher, M.A. Fillol, A.M. Andrews, Simultaneous serotonin and dopamine monitoring across timescales by rapid pulse voltammetry with partial least squares regression, Anal. Bioanal. Chem. 413 (2021) 6747–6767.
[24] D. Das, D. Biswas, A.K. Hazarika, S. Sabhapondit, R.B. Roy, B. Tudu, R. Bandyopadhyay, Cuo nanoparticles decorated MIP-based electrode for sensitive determination of gallic acid in green tea, IEEE Sensors J. 21 (5) (2020) 5687–5694.
[25] G.H. Matsushita, L.E. Oliveira, A.H. Sugi, C. da Cunha, Y.M. Costa, Automatic identification of phasic dopamine release, in: 2018 25th International Conference on Systems, Signals and Image Processing, IWSSIP, IEEE, 2018, pp. 1–5.
[26] J. Massah, K.A. Vakilian, An intelligent portable biosensor for fast and accurate nitrate determination using cyclic voltammetry, Biosyst. Eng. 177 (2019) 49–58.
[27] X. Zhang, J. Zhang, Y. Cai, S. Xu, H. Wu, X. Chen, Y. Huang, F. Li, Integrated electrochemical aptasensor array toward monitoring anticancer drugs in sweat, Anal. Chem. 96 (12) (2024) 4997–5005.
[28] X. Zhang, Y. Tang, H. Wu, Y. Wang, L. Niu, F. Li, Integrated aptasensor array for sweat drug analysis, Anal. Chem. 94 (22) (2022) 7936–7943.
[29] S. Balakrishnama, A. Ganapathiraju, Linear discriminant analysis-a brief tutorial, Inst. Signal Inf. Process. 18 (1998) (1998) 1–8.
[30] S.S. Abolmaali, A.M. Tamaddon, R. Dinarvand, A review of therapeutic challenges and achievements of methotrexate delivery systems for treatment of cancer and rheumatoid arthritis, Cancer Chemother. Pharmacol. 71 (2013) 1115–1130.
[31] R.M. Mader, B. Rizovski, G.G. Steger, A. Wachter, R. Kotz, H. Rainer, Exposure of oncologic nurses to methotrexate in the treatment of osteosarcoma, Arch. Environ. Health: An Int. J. 51 (4) (1996) 310–314.
[32] A.S. Steijlen, M. Parrilla, R. Van Echelpoel, K. De Wael, Dual microfluidic sensor system for enriched electrochemical profiling and identification of illicit drugs on-site, Anal. Chem. 96 (1) (2023) 590–598.
[33] L.-C. Tai, W. Gao, M. Chao, M. Bariya, Q.P. Ngo, Z. Shahpar, H.Y. Nyein, H. Park, J. Sun, Y. Jung, et al., Methylxanthine drug monitoring with wearable sweat sensors, Adv. Mater. 30 (23) (2018) 1707442.
[34] R. Van Echelpoel, M. de Jong, D. Daems, P. Van Espen, K. De Wael, Unlocking the full potential of voltammetric data analysis: A novel peak recognition approach for (bio) analytical applications, Talanta 233 (2021) 122605.
[35] J. Alva-Ensastegui, E. Morales-Avila, A.P. de la Luz, M. Bernad-Bernad, Determination of pka values and deprotonation order of methotrexate using a combined experimental-theoretical study and binding constants of the methotrexate-laponite complex at different pH values, J. Photochem. Photobiol. A: Chem. 449 (2024) 115406.
[36] H. Mark, C.R. Harding, Amino acid composition, including key derivatives of eccrine sweat: potential biomarkers of certain atopic skin conditions, Int. J. Cosmet. Sci. 35 (2) (2013) 163–168.
[37] L.B. Baker, Physiology of sweat gland function: The roles of sweating and sweat composition in human health, Temperature 6 (3) (2019) 211–259.
[38] L.B. Baker, A.S. Wolfe, Physiological mechanisms determining eccrine sweat composition, Eur. J. Appl. Physiol. 120 (2020) 719–752.